# Kinematic effects in the Debye–Waller factor and sticking probabilities in low-energy atom–surface scattering

**Antonio Šiber[1], Branko Gumhalter[1,2,4] and Christof Wöll[3]**

[1] Institute of Physics of the University, PO Box 304, 10001 Zagreb, Croatia
[2] Donostia International Physics Centre (DIPC), 20018 San Sebastián, Basque Country, Spain
[3] Ruhr-Universität Bochum, Lehrstuhl für Physikalische Chemie I, D-44801 Bochum, Germany

E-mail: branko@ifs.hr

## Abstract
We present a theoretical analysis of kinematic effects that may strongly influence the magnitude of Debye–Waller factors and inelastic reflection and sticking coefficients describing thermal energy inert-gas-atom scattering from surface phonons. Assessment of the effects discussed is carried out for inelastic helium-atom scattering (HAS) from adsorbed Xe monolayers whose vibrational properties have been extensively studied in recent HAS experiments.

## 1. Introduction

Various kinematic effects can strongly influence the magnitude of inelastic scattering probabilities in atom–surface scattering. One of the most widely discussed effects of this kind is the phenomenon of kinematic focusing of inelastically scattered beams [1] which was first discussed in connection with the early theoretical interpretations of experimental data from the fast-growing field of helium-atom scattering (HAS) from surface phonons [2]. Since then, quite a few manifestations of the kinematic focusing effects in inelastic He-atom-scattering time-of-flight (HAS TOF) spectra have been reported in the literature [3–6]. Theoretical aspects of the various resonance and focusing effects which may act to enhance the scattered beam intensity in specific scattering directions and for particular energy and parallel momentum transfers have also been extensively studied and reviewed [7–13].

A typical example of strong kinematic effects in HAS TOF spectroscopy of surface phonons [1] that is frequently cited in the introductory literature on HAS from surfaces [14,16] pertains to the enhancement of measured one-phonon spectral peak intensities that are associated with directional focusing of the scattered beam current. This phenomenon was observed and can be most easily interpreted in the in-sagittal-plane scattering geometry in

---

[4] Author to whom any correspondence should be addressed.

which the initial and final projectile momenta $K_i$ and $K_f$, respectively, lie in the same plane normal to the surface. In this case the relation between the energy transfer, $\Delta E = E_f - E_i$, and the parallel momentum transfer, $\Delta K = K_f - K_i$, to phonons, the so-called scan curve $\Delta E = \Delta E(\Delta K)$, acquires a particularly simple form. This enables a relatively straightforward assessment of the dispersion of surface phonons to be made by comparing the values of $\Delta E$ and $\Delta K$ corresponding to the one-phonon TOF spectral peaks with the values obtained from intersections of the dispersion curve calculated for a $j$th phonon mode branch, $\omega_{\Delta K, j}$, and the scan curve for a given scattering geometry [14]. Hence, the following introductory illustration of the most frequent kinematic focusing effect will be restricted to the case of the in-sagittal-plane scattering geometry as this is also the most relevant to experimental situations.

Using TOF spectroscopy one can detect just the projectile particles whose initial and final states are the genuine scattering states, with the asymptotic forms of the incoming and outgoing wavefunctions that approach plane waves far outside the surface, and are hence characterized by the well-defined wavevectors $k_i = (K_i, k_{zi})$ and $k_f = (K_f, k_{zf})$, respectively. In terms of these quantum numbers the projectile initial and final energies are respectively given by

$$E_i = \frac{\hbar^2 K_i^2}{2M} + \frac{\hbar^2 k_{zi}^2}{2M}, \qquad E_f = \frac{\hbar^2 K_f^2}{2M} + \frac{\hbar^2 k_{zf}^2}{2M}. \tag{1}$$

The corresponding scan curve for in-sagittal-plane scattering is expressed as

$$\Delta E(\Delta K) = E_f - E_i = \frac{\hbar^2}{2M}\left(\frac{|K_i + \Delta K|^2}{\sin^2 \theta_f} - k_i^2\right), \tag{2}$$

where $M$ is the projectile mass and $\theta_f$ denotes the final scattering angle relative to the surface normal. In the majority of TOF measurements carried out in the sagittal plane, the total scattering angle $\theta_{SD} = \theta_i + \theta_f$, where $\theta_i$ is the incident angle, is kept fixed for practical purposes, so $|\Delta K|$ is uniquely determined from the values of $|k_i|$, $\theta_i$, and $\Delta E$.

The surface-localized Rayleigh wave (RW) and longitudinal resonance (LR) phonons [15] couple most strongly to the scattered He atoms and hence the effects of kinematic focusing have been dominantly discussed in connection with the RW and LR spectral weights in the measured TOF spectra. To illustrate the origin of the most frequently discussed case of kinematic focusing associated with exchange of surface phonons, we note that the one-phonon excitation intensities, as occurring in the measured spectra of inelastically scattered atoms, should be proportional to a segment of the phase space of allowed *final-state* quantum numbers, i.e. the wavevectors $k_f$, of the projectile. Since the experimental TOF spectra are *energy and angle resolved* they are integrated over all projectile final parallel wavevectors satisfying the energy conservation in the scattering geometry of the experiment. This means that the energy-conserving $\delta$-functions appearing in theoretical expressions for the probabilities of state-to-state projectile transitions involving one-phonon emission or absorption processes [14, 16, 17] should be transformed so as to enable integration over the allowed parallel momentum transfers confined to the scan curve [1, 14]; that is,

$$\delta(\Delta E(\Delta K) \pm \hbar\omega_{\Delta K, j})\, \mathrm{d}(\Delta E)$$

$$\rightarrow \sum_{\Delta K_j} \frac{\partial \Delta E(\Delta K)}{\partial \Delta K}\left(\frac{\partial \Delta E(\Delta K)}{\partial \Delta K} - \frac{\partial \hbar\omega_{\Delta K, j}}{\partial \Delta K}\right)^{-1} \delta(\Delta K - \Delta K_j)\, \mathrm{d}(\Delta K). \tag{3}$$

Here $\Delta K_j$ denote the points of intersection of the scan curve with the $j$th-phonon-branch dispersion curve. When two such intersections coalesce, i.e. when the scan curve osculates the phonon dispersion curve, the factor multiplying the $\delta$-function on the RHS of expression (3) becomes singular. The singular behaviour can be evaluated for particular $\Delta E(\Delta K)$ and $\hbar\omega_{\Delta K, j}$

dependences and scattering geometries [1, 14] and thereby the maxima in the scattering spectra originating from this particular mechanism of kinematic focusing can be predicted [1, 3, 4] and distinguished from *other* resonance and kinematic effects in atom–surface scattering [5, 6, 12].

The situation concerning the relevance of scattering geometry becomes more complex if after the collision the projectile may remain *localized at the surface* in one of the bound states of the static projectile–surface potential. This may occur either in selective adsorption processes in which the energy of perpendicular projectile motion is converted into the energy of motion parallel to the surface due to the exchange of a reciprocal-lattice vector $G$ with the crystal [2, 7], or in phonon-mediated processes in which a sufficient amount of the projectile perpendicular energy is transferred to excite or absorb phonons that the projectile remains localized or stuck in one of the bound states $|n\rangle$ of the perpendicular atom–surface potential (for a review on the theoretical descriptions of sticking processes see [18, 19] and references therein). The expression describing the change of projectile energy after making a transition into a bound state with perpendicular energy $\epsilon_n < 0$ reads

$$\Delta E(\Delta K) = E_f - E_i = \frac{\hbar^2 (K_i + \Delta K)^2}{2M} + \epsilon_n - \frac{\hbar^2 k_i^2}{2M}. \tag{4}$$

Here we shall avoid associating the term 'scan curve' with the $\Delta E(\Delta K)$ dependence in expression (4) because the transitions into bound states are not measured by the TOF spectroscopy and therefore the projectile parallel momentum appearing in equation (4) need not be confined to the sagittal plane for any detection purposes.

In prompt or one-step sticking processes the requirement that $\Delta K$ and $\Delta E$ obey the parallel momentum and energy conservation in one-phonon exchange may introduce quite new features in the scattering events, including manifestations of the various resonance and focusing effects that may give rise to extrema in inelastic transition probabilities. In the following sections we shall discuss kinematic effects that may strongly influence the probabilities of inelastic reflection and sticking processes which are characterized by very low projectile incident energies of the order of the well depth of the projectile–surface potential. These probabilities constitute and determine the magnitude of the Debye–Waller factor (DWF) (or factors) which give an overall measure of inelasticity of the scattering event in the quantum regime. Since a detailed knowledge of the magnitude and properties of the DWF represents a prerequisite for a general understanding of the phonon-assisted inelastic scattering and sticking at very low incident energies, we shall study its behaviour as a function of kinematic parameters that define the characteristics of the incident beam.

In section 2 we present the essentials of a theoretical formalism which enables a full quantum mechanical treatment of inelastic scattering of inert-gas atoms from surface phonons. We pay special attention to inelastic transitions leading to prompt sticking and discuss general conditions in which the sticking mediated by excitation of phonons with Einstein- or Debye-like dispersion may be affected by the focusing effects in final-state scattering channels. In section 3 we give an overview of the HAS studies and theoretical interpretations of vibrational properties of the prototype system Xe/Cu(111) which supports Einstein- and Debye-like surface phonons and hence is ideally suited for the analyses of the aforementioned focusing phenomena. In section 4 we analyse the conditions under which inelastic scattering of He atoms from and sticking on the Xe/Cu(111) surface can be strongly affected by kinematic factors and focusing processes. The main conclusions of these analyses are summarized in section 5.

## 2. Description of inelastic atom–surface scattering and sticking in the scattering spectrum formalism

Complete information on the inelastic reflection and sticking processes and the DWF in HAS can be obtained from the expression for the energy- and parallel-momentum-resolved scattering

spectrum $N_{k_i,T_s}(\Delta E, \Delta K)$. This expression gives the probability density that an inert atom incident on a surface with momentum $\hbar k_i$ exchanges an amount of energy $\Delta E$ and parallel momentum $\Delta K$ in interaction with the phonons of the target [16, 22] that is in thermal equilibrium at the temperature $T_s$. For the scattering conditions typical of thermal energy HAS experiments, the uncorrelated phonon exchange processes dominate over the correlated ones [16, 22] and the latter can be neglected to a very good approximation. In this regime the scattering spectrum can be accurately calculated using the exponentiated Born approximation (EBA) scattering formalism [16, 20–22]. This yields the EBA scattering spectrum [22]:

$$N_{k_i,T_s}^{EBA}(\Delta E, \Delta K) = \int_{-\infty}^{\infty} \frac{\mathrm{d}\tau\, \mathrm{d}^2\mathcal{R}}{(2\pi\hbar)^3}\, \mathrm{e}^{(\mathrm{i}/\hbar)[(\Delta E)\tau - \hbar(\Delta K)\mathcal{R}]} \exp[2W_{k_i,T_s}^{EBA}(\mathcal{R}, \tau) - 2W_{k_i,T_s}^{EBA}(0,0)],$$
(5)

where $\tau$ and $\mathcal{R} = (X, Y)$ are the variables of the so-called EBA scattering or driving function $2W_{k_i,T_s}^{EBA}(\mathcal{R}, \tau)$, explicitly given below (cf equation (7)), which contains all the information on uncorrelated phonon exchange processes in an atom–surface scattering event. After carrying out the $(\tau, \mathcal{R})$ Fourier transform on the RHS of equation (5), the values of $\Delta K$ and $\Delta E$ should be confined to the scan curve for a given scattering geometry, usually for fixed scattering angles $\theta_i$ and $\theta_f$ in a particular experiment. This yields the desired theoretical intensities as a function of $\Delta E$ and $\Delta K$ which can be directly compared with the experimental HAS TOF intensities [16]. Here we have assumed a monoenergetic and monodirectional incident beam of atoms whose motion is described by plane waves, because in the following sections we shall focus the discussion on kinematic effects that can give rise to extrema in the total scattering and sticking probabilities defining the DWF. Since these probabilities are obtained by integration over all open final-state scattering channels without any restriction on the scattering geometry embodied in the scan curves, the representation of the incident beam by a monochromatic plane wave is a good approximation in view of the $k_i$-dependence of the integrated quantities that characterize the scattering system (see also the discussion at the end of this section). However, in the comparisons of experimental energy- and angle-resolved HAS TOF spectra with those calculated using expression (5), we shall convolute the theoretical spectra with a Gaussian that models the overall energy resolution of the TOF apparatus in a particular measurement.

The quantity $2W_{k_i,T_s}^{EBA}(\mathcal{R} = 0, \tau = 0) = 2W_{k_i,T_s}^{EBA}$ in equation (5) gives the EBA expression for the Debye–Waller exponent (DWE) characteristic of the inelastic scattering spectrum studied [16]. It has also been shown [21] that this DWE represents the mean number of phonons, $\bar{n}$, excited in all inelastic scattering events characterized by the projectile initial momentum $\hbar k_i$ and the substrate temperature $T_s$. The corresponding DWF given by $\exp[-2W_{k_i,T_s}^{EBA}] = \mathrm{e}^{-\bar{n}}$ represents, according to equation (5), a common attenuating factor for all the spectral features in $N_{k_i,T_s}^{EBA}(\Delta E, \Delta K)$ for particular initial conditions ($k_i$ and $T_s$). The spectrum (5) also includes the elastically scattered specular beam intensity that is given by [23]:

$$(N_{k_i,T_s}^{EBA}(\Delta E, \Delta K))_{\text{specular}} = \mathrm{e}^{-2W_{k_i,T_s}^{EBA}}\delta(\Delta E)\delta(\Delta K).$$
(6)

In the present description in which we assume a statically flat surface and linear projectile–phonon coupling [12, 16, 22], the EBA scattering function in equation (5) takes the form:

$$2W_{k_i,T_s}^{EBA}(\mathcal{R}, \tau) = \sum_{Q,G,j,k_z'} [|\mathcal{V}_{k_z',k_{zi}}^{K_i, Q+G, j}(+)|^2 [n(\hbar\omega_{Q,j}) + 1]\mathrm{e}^{-\mathrm{i}(\omega_{Q,j}\tau - (Q+G)\mathcal{R})}$$
$$+ |\mathcal{V}_{k_z',k_{zi}}^{K_i, Q+G, j}(-)|^2 n(\hbar\omega_{Q,j})\mathrm{e}^{\mathrm{i}(\omega_{Q,j}\tau - (Q+G)\mathcal{R})}].$$
(7)

Here $Q$ denotes the phonon wavevector in the first surface Brillouin zone (SBZ), $n(\hbar\omega_{Q,j})$ is the Bose–Einstein distribution of phonons of energy $\hbar\omega_{Q,j}$ at the target temperature $T_s$, and the summation over projectile final-state quantum numbers $k_z'$ describing the motion

in the $z$-direction is carried out over the continuum states $|k'_z\rangle$ for which $E_{k'_z} = E_{zf} = (\hbar k_{zf})^2/2M > 0$, and the bound states $|n\rangle$ of the static projectile–surface potential $U_0(z)$ for which $E_{k'_z} = E_{zf} = \epsilon_n < 0$. The one-phonon emission (+) and absorption (−) scattering probabilities $|\mathcal{V}_{k'_z,k_{zi}}^{K_i,Q+G,j}(\pm)|^2$ are calculated from the projectile–phonon interaction matrix elements $V_{k'_z,k_{zi}}^{K_i,K_i\pm Q\pm G,j}$ following the rule [16, 22]

$$|\mathcal{V}_{k'_z,k_{zi}}^{K_i,Q+G,j}(\pm)|^2 = |2\pi V_{k'_z,k_{zi}}^{K_i,K_i\mp Q\mp G,j}\delta(E_f - E_i \pm \hbar\omega_{Q,j})|^2. \tag{8}$$

Now, depending on whether the final energy of the projectile motion perpendicular to the surface belongs to the continuous part of the spectrum, $E_{zf} = (\hbar k_{zf})^2/2M > 0$, or to the discrete spectrum, $E_{zf} = \epsilon_n < 0$, the singular energy-conserving $\delta$-function on the RHS of expression (8) should be appropriately treated and converted into a nonsingular expression so as to enable summations over the final-state quantum numbers in expression (7).

In the case of continuum-to-continuum (c–c) inelastic transitions of the projectile, the transformation of the RHS of expression (8) is performed according to [16, 22]

$$|2\pi V_{k'_z,k_{zi}}^{K_i,K_i\mp Q\mp G,j}\delta(E_{K_i\mp Q\mp G,k'_z} - E_{K_i,k_{zi}} \pm \hbar\omega_{Q,j})|^2$$

$$= \frac{1}{\hbar^2}\left|\frac{V_{k'_z,k_{zi}}^{K_i,K_i\mp Q\mp G,j}}{\sqrt{j_{zi}j'_z}}\right|^2 \delta_{k'_z,k_z(\pm)}\Theta(k_z^2(\pm)), \tag{9}$$

where $\Theta(x)$ is the Heaviside step function, $\delta_{k'_z,k_z}$ is the Kronecker symbol, and

$$k_z^2(\pm) = \frac{2M}{\hbar^2}(E_{K_i} + E_{k_{zi}} - E_{K_i\mp Q\mp G} \mp \hbar\omega_{Q,j}), \tag{10}$$

where the projectile currents normal to the surface in the entrance and inelastic scattering channels are given by $j_{zi} = v_{zi}/L_z$ and $j'_z = v_{fz}/L_z$, respectively, $v_z = \hbar k_z/M$, and $L_z$ denotes the quantization length in the $z$-direction. The conversion expressed through equation (9) enables the summations over $(Q, G, k'_z)$ in equation (5) to be easily carried out, whereby all quantization lengths cancel out from the final expression [14, 16, 22]. For the specific case of He $\rightarrow$ Xe/Cu(111) collisions studied in the following sections, the calculation of the projectile–phonon matrix elements $V_{k'_z,k_z}^{K_i,K_i\mp Q\mp G,j}$ in terms of two-dimensional Fourier transforms $v_Q(z)$ of pairwise He-adsorbate potentials, $v(r)$, has been illustrated and discussed in detail in [12], and here we only quote the result:

$$V_{k'_z,k_{zi}}^{K_i,Q+G,j} = \left(\frac{\hbar}{2NM_{\text{Xe}}\omega_{Q,j}}\right)^{1/2}$$

$$\times \int dz\, \chi_f^*(z)e_\kappa(Q,j)\cdot\left[-i(Q+G),\hat{z}\frac{\partial}{\partial z}\right]v_{Q+G}(z-z_\kappa)\chi_i(z). \tag{11}$$

Here $M_{\text{Xe}}$ is the mass of the adsorbate Xe atom, $z_\kappa$ is the $z$-coordinate of the Xe atoms in the adlayer, $e_\kappa(Q,j)$ is the polarization vector of the $(Q,j)$th phonon mode localized in the adlayer, $\hat{z}$ denotes the unit vector perpendicular to the surface, and $\chi_{i,f}(z)$ are the $z$-components of the initial- and final-state wavefunctions of a He atom moving in the static projectile–surface potential $U_0(z)$.

In the case of the continuum-to-bound (c–b) state inelastic transitions of the projectile, the RHS of expression (8) is transformed so that the summation over final-state quantum numbers $n$ of the discrete bound states of the projectile–surface potential is performed according to [16]

$$\sum_n(\cdots)|2\pi\delta(E_{K_i-Q-G} + \epsilon_n \pm \hbar\omega_{Q,j} - E_{k_i})|^2$$

$$\rightarrow \sum_n(\cdots)\frac{2\pi}{\hbar j_{zi}}\delta(E_{K_i-Q-G} + \epsilon_n \pm \hbar\omega_{Q,j} - E_{k_i}). \tag{12}$$

Concerning the kinematics of sticking transitions that affect the behaviour of the argument of the energy-conserving $\delta$-function in equation (12), we observe that in expressions (4) and (12) both cases $E_f - E_i < 0$ and $E_f - E_i > 0$ are kinematically allowed. However, in the following discussions we shall restrict our attention to the prompt sticking processes in which the energy is transferred from the projectile to the target phonons such that the total change of the projectile energy is negative, i.e. $E_f - E_i < 0$. The transitions for which $E_f - E_i > 0$ are less probable at low surface temperature and render highly unstable final states that—due to the strong coupling of phonons to a projectile moving parallel to the surface—will very quickly decay via phonon emission into the ones for which the change of the total projectile energy is negative. These correlated processes are of higher order in the coupling constant and the number of exchanged phonons than the sticking processes involving one-phonon emission and satisfying $E_f - E_i < 0$. As the latter processes are dominant at low temperatures, we shall not consider the case $E_f - E_i > 0$ in the following treatment of kinematic effects associated with one-phonon-assisted sticking transitions. It should also be noted that in one-dimensional scattering models and in three-dimensional scattering models with zero parallel momentum transfer, all the one-phonon-assisted prompt sticking transitions satisfy the condition $E_f - E_i < 0$.

The total EBA scattering function, $2W^{EBA}_{k_i, T_s}(\tau, \mathcal{R})$, that includes the prompt sticking processes with $E_f - E_i < 0$ is obtained by combining the expression $2W^{c \to c}_{k_i, T_s}(\tau, \mathcal{R})$, which encompasses the contributions from c–c transitions $|k_{zi}\rangle \to |k'_z\rangle$, with the term

$$2W^{c-b}_{k_i, T_s}(\tau, \mathcal{R}) = \frac{2\pi}{\hbar j_{zi}} \sum_{Q, G, j, n} |V^{K_i, K_i - Q - G, j}_{n, k_{zi}}|^2 \delta(E_{K_i - Q - G} + \epsilon_n + \hbar\omega_{Q, j} - E_{k_i})$$

$$\times [n(\hbar\omega_{Q, j}) + 1] e^{-i[\omega_{Q, j}\tau - (Q + G)\mathcal{R}]}, \tag{13}$$

which describes the contribution from one-phonon-emission-assisted c–b transitions $|K_i, k_{zi}\rangle \to |K_i - Q - G, n\rangle$ for which $E_f < E_i$. Hence, only the term containing the factor $[n(\hbar\omega_{Q, j}) + 1]$ appears on the RHS of equation (13).

Analogously, we find for the total DWE

$$2W^{EBA}_{k_i, T_s} = 2W^{c \to c}_{k_i, T_s} + 2W^{c-b}_{k_i, T_s}, \tag{14}$$

where the prompt sticking correction $2W^{c-b}_{k_i, T_s} = 2W^{c-b}_{k_i, T_s}(\tau = 0, \mathcal{R} = 0)$ may represent a significant contribution to the total DWE at low projectile incoming energies. As we shall show in section 3, in the scattering regime in which the magnitude of $E_i$ is comparable to the projectile–surface potential well depth, the total probability for projectile transitions into the bound states increases such that it may become comparable with or even exceed the total probability for inelastic scattering into the continuum states (cf figure 9). Hence, in the applications of the EBA formalism to calculate the DWF in the low-energy scattering regime, it is essential to take into account the prompt sticking contribution given by the second term on the RHS of equation (14).

The total sticking probability for the projectile with incoming energy $E_i$, or the prompt sticking coefficient, is then given by

$$s_{k_i, T_s} = \int_{-\infty}^{-E_i} d(\Delta E) \int d^2(\Delta K)\, N_{k_i, T_s}(\Delta E, \Delta K), \tag{15}$$

from which $s^{EBA}_{k_i, T_s}$ is obtained by substituting the EBA scattering spectrum (5) on the RHS of equation (15). Here it should be reiterated that the scattering function (7), the total DWE (14) deriving from it, and the prompt sticking coefficient (15) are obtained by summation (integration) over the quantum numbers of all open inelastic scattering channels. Therefore these quantities describe integrated or global characteristics of the collision system that can depend only on the kinematic parameters of the incident beam and the substrate temperature.

Now, it is apparent from the structure of the expression on the RHS of equation (13) that a singular character of the energy-conserving $\delta$-function can give rise to maxima in the summed-over or integrated expression for the sticking component of the total scattering function (7) for specific values of the kinematic parameters, namely the incident angle and momentum of the projectile. This can be easily illustrated on a simple example of Einstein and Debye models of surface phonon frequency entering the argument of the $\delta$-function on the RHS of equation (13).

Assuming first the Einstein type of dispersion in expression (13), namely $\omega_Q = \omega_0 = $ constant, and taking into account that the summation is carried out over the quasi-continuum of $Q$-values, we can conveniently represent the $\delta$-function on the RHS of equation (12) for the case $G = 0$ in the form

$$\delta(E_{K_i - Q} + \epsilon_n + \hbar\omega_0 - E_{k_i}) = \frac{2M}{\hbar^2}\delta(Q^2 - 2QK_i\cos\varphi - k_{zi}^2 + 2M(\hbar\omega_0 + \epsilon_n)/\hbar^2), \qquad (16)$$

where $\varphi$ is the polar (in-surface-plane) angle between the vectors $K_i$ and $Q$. By equating the argument of the $\delta$-function on the RHS of equation (16) with zero, one obtains a quadratic equation in $Q$ whose solutions are

$$Q_{\pm} = K_i\cos\varphi \pm \sqrt{(K_i\cos\varphi)^2 + [k_{zi}^2 - 2M(\hbar\omega_0 + \epsilon_n)/\hbar^2]}. \qquad (17)$$

These solutions are real if the discriminant

$$D(k_i, \varphi, n) = (K_i\cos\varphi)^2 + [k_{zi}^2 - 2M(\hbar\omega_0 + \epsilon_n)/\hbar^2] \qquad (18)$$

is positive or zero. Using these definitions we can transform the energy-conserving $\delta$-function to the form

$$\delta(E_{K_i - Q} + \epsilon_n + \hbar\omega_0 - E_{k_i}) = C[\alpha_+(k_i, \varphi, n)\delta(Q - Q_+) + \alpha_-(k_i, \varphi, n)\delta(Q - Q_-)], \qquad (19)$$

where $C$ is a constant depending on the units in which the energies and wavevectors are measured, and

$$\alpha_{\pm}(k_i, \varphi, n) = \frac{\Theta(D(k_i, \varphi, n))\Theta(Q_{\pm})}{2\sqrt{D(k_i, \varphi, n)}}. \qquad (20)$$

Now, it is seen that expression on the RHS of equation (19) can give rise to singularities or maxima in the sticking component of the scattering function and the DWE whenever either of $\alpha_{\pm}(k_i, \varphi, n)$ becomes singular or large for specific values of the kinematic parameters that define the scattering conditions. This is illustrated in figure 1 in which $\alpha_+(k_i, \varphi, n)$ is shown as a function of $k_i$ and $\varphi$ characteristic of the scattering conditions in He $\rightarrow$ Xe/Cu(111) experiments described below. Thus, for incident scattering angle $\theta_i = 50°$ the quantity $\alpha_+(k_i, \varphi, n)$ exhibits singular behaviour in a limited segment of the $(k_i, \varphi)$ phase space (cf figure 1(a)) which may give rise to focusing effects that act so as to enhance the prompt sticking events in restricted intervals of *final-state quantum numbers* over which the summation in expression (13) is carried out. Such features are reflected in the exchange of phonons with wavevectors pointing in the azimuthal direction defined by the location of maxima of $\alpha_{\pm}(k_i, \varphi, n)$. On the other hand, at normal incidence $\theta_i = 0$ all azimuthal directions are equally preferred as regards the kinematic parameters of the incident atom (cf figure 1(b)) and the only discrimination among the various directions may then arise if there exists an anisotropy in other factors entering the interaction matrix elements and the scattering function.

A very similar simple analysis can be also made for the Debye model of dispersion $\omega_Q = cQ$ in expression (13). Like in the case of Einstein dispersion, the argument of the energy-conserving $\delta$-function in the expression on the RHS of equation (13) gives rise to a quadratic equation with solutions $Q_{\pm}$ in terms of which the $\delta$-function can be expressed in the $Q$-space, in a fashion analogous to equation (19). Again as in the case of Einstein

(a)



(b)
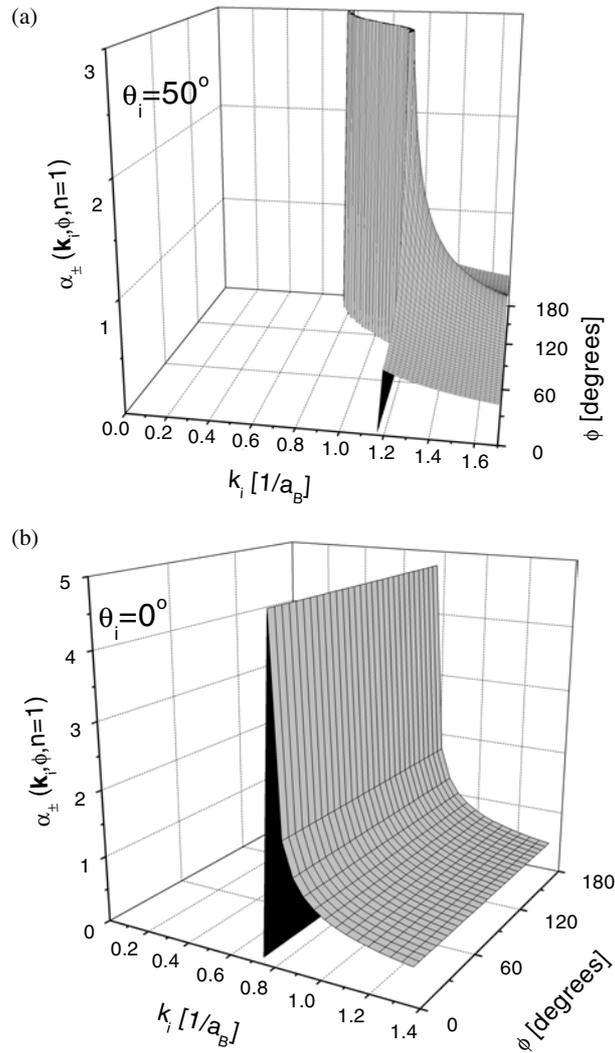


**Figure 1.** Plots of $\alpha_+(k_i, \varphi, n = 1)$ (cf equation (20)), corresponding to the He-atom transition into a bound state $\epsilon_{n=1} = -1.551$ meV of the static He–Xe/Cu(111) model potential [25] through emission of an Einstein phonon of energy $\hbar\omega_0 = 2.62$ meV. The magnitude of the incident wavevector $|k_i|$ is measured in inverse bohrs $a_B^{-1}$ (atomic units). The angle of incidence of the He atom in (a) is $\theta_i = 50°$ relative to the surface normal, and in (b) $\theta_i = 0°$.

phonon dispersion, the prefactors $\alpha_\pm(k_i, \varphi, n)$ calculated for the Debye dispersion may exhibit maxima in some segments of the phase space of kinematic parameters and thereby give rise to *preferential prompt sticking transitions into restricted intervals of final-state quantum numbers*. Calculations in which this effect proved important were carried out for the RW-mediated sticking of noble-gas atoms on a Cu(111) surface [24]. Here we show in figure 2(a) the behaviour of $\alpha_+(k_i, \varphi, n)$ for the Debye model of dispersion of the RW characteristic of the Xe(111) surface for $\theta_i = 50°$ (the value of $\alpha_-(k_i, \varphi, n)$ is equal to zero for the scattering conditions considered). By contrast, for angle of incidence $\theta_i = 0$ there is no preferential direction for wavevectors of emitted Debye phonons (cf figure 2(b)), in complete analogy with the case of Einstein phonons.

(a)



(b)
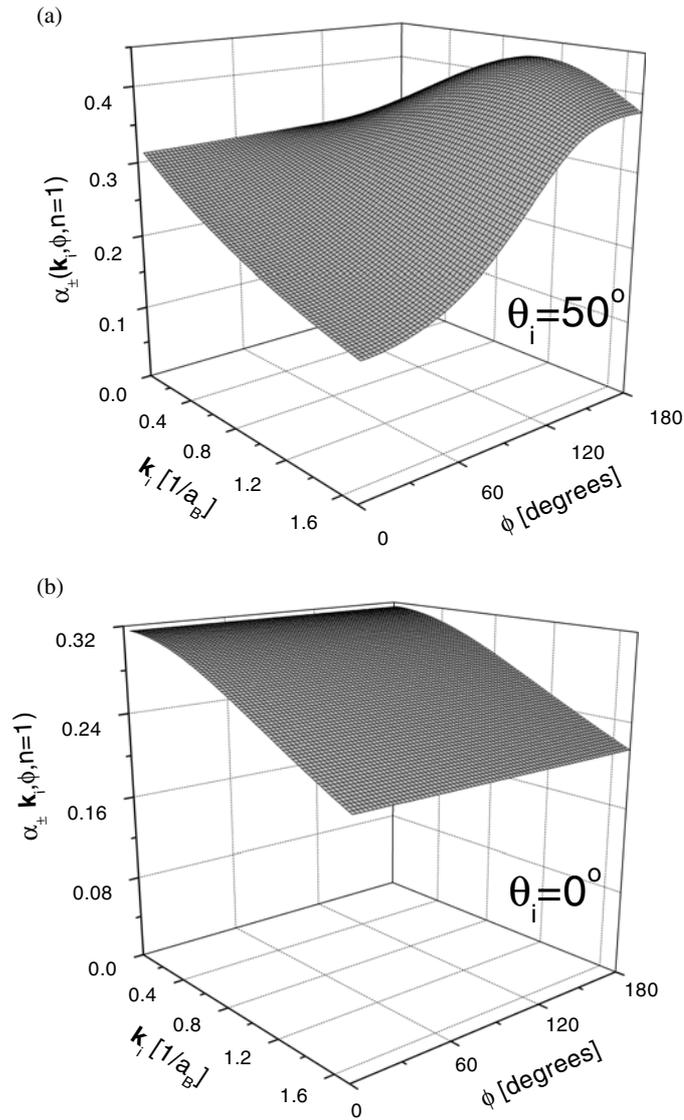


**Figure 2.** A plot of $\alpha_+(k_i, \varphi, n = 3)$ corresponding to the He-atom transition into a bound state $\epsilon_{n=3} = -0.095$ meV of the static He–Xe(111) model potential [12] through emission of a Debye-like surface phonon with sound velocity $c = 6.46(a_B/\hbar)$ meV. The magnitude of the incident wavevector $|k_i|$ is measured in inverse bohrs $a_B^{-1}$ (atomic units). The angle of incidence of the He atom is $\theta_i = 22.5°$ in (a) and $\theta = 0°$ in (b).

In the present description of atom–surface scattering the impinging beam of atoms has been assumed monochromatic and monodirectional so that the projectile motion was described by a single quantum number $k_i$ appropriate to an incoming plane wave. That is, the singular character of the functions $\alpha_\pm(k_i, \varphi, n)$ defined in equation (20) is relevant here in connection with the range of final-state quantum numbers over which the summation (integration) in expression (7) is carried out. As this range substantially exceeds the energy and angular resolution of the HAS TOF apparatus, no summation or averaging over the initial projectile states $|k_i\rangle$ was included in the calculation of the scattering spectrum (5). On the other hand, for

incident beams appropriately described by wavepackets with a finite spread of the initial-state wavevector, such summations may become necessary in the interpretation of HAS TOF spectra that are energy and angle resolved in the *exit* channels and hence may be strongly affected by the focusing effects that depend on the beam characteristics in the *entrance* channel. The type of focusing effects arising in connection with the angular spread of the incident beam and their consequences for the sticking processes have been discussed in [13]. These effects are complementary to the ones briefly illustrated above and should also be included in quantitative interpretations of the energy- and angle-resolved HAS TOF spectra involving incident beams with finite energy and angular spread.

## 3. A monolayer of Xe atoms on Cu(111): the prototype system for studying dispersive and nondispersive surface phonons

Benchmark examples of systems that support nondispersive (Einstein-like) and dispersive surface phonons are realized by adsorption of monolayers of Xe atoms on three low-index Cu crystal surfaces (for an exhaustive list of references see [16]). Since these systems have been extensively studied and characterized by the various surface science techniques, they naturally lend themselves to analyses of the role that a combination of kinematic factors and phonon excitations may play in atom–surface scattering. In the following we shall restrict our attention to the system Xe/Cu(111).

The various aspects of HAS studies of the commensurate monolayer system ($\sqrt{3} \times \sqrt{3}$)R30° Xe/Cu(111) at a substrate temperature around $T_s = 60$ K have been reported in [25–28]. Earlier experiments revealed Xe adsorption on top of Cu atoms [29] for the commensurate Xe monolayer structure [30] that is stable above 48 K at which the incommensurate–commensurate structural phase transition takes place [31].

The right-hand side panel in figure 3(*a*) shows the structure of the commensurate ($\sqrt{3} \times \sqrt{3}$)R30° monolayer of Xe atoms adsorbed on Cu(111) [29, 30] and indicates the two principal directions (azimuths) of the substrate crystal surface. The left-hand-side panel shows the first SBZ of the substrate (dashed lines) and the two-dimensional BZ of the adlayer (full lines). Figure 3(*b*) shows an angular distribution of He atoms scattered from the ($\sqrt{3} \times \sqrt{3}$)R30° Xe/Cu(111) surface for incident wavevector $k_i = 9.2$ Å$^{-1}$ ($E_i = 45$ meV) and the substrate temperature $T_s = 60$ K along the [1$\bar{1}$0] azimuth relative to the substrate surface. The intensities are normalized to the specular peak height. In addition to the $(1, 0)$ diffraction peak, two additional, Xe $(1/3, 0)$ and $(2/3, 0)$ diffraction peaks of order one third were observed [26]. The sharpness of the peaks and relatively low background indicate the presence of a well-ordered, largely defect-free Xe overlayer. Hence, the Xe adlayer may be considered planar and periodic with hexagonal symmetry and this is then reflected in its vibrational properties. The adlayer vibrational modes can be classified as dominantly in-plane polarized (longitudinal (L) and shear horizontal (SH)) and shear vertical (S) [32]. The planar character and the flatness of the Xe adlayer (from the viewpoint of He–surface interaction) make possible the application of the theoretical model developed in the preceding section to interpret the measured TOF spectra as well as to analyse the effects of kinematic factors on the quantities such as the DWFs and sticking probabilities.

Figure 4 shows typical He-atom TOF spectra for the ($\sqrt{3} \times \sqrt{3}$)R30° Xe/Cu(111) surface along the [11$\bar{2}$] substrate azimuth (i.e. along the $\bar{\Gamma}\bar{K}_{Xe}$ direction of the superstructure), for three different He-atom incident energies spanning the transition from a single- to a multi-quantum scattering regime. The spectrum at the lowest incident energy ($E_i = 9.9$ meV) is typical of a single-phonon scattering regime and is dominated by two well-defined peaks at $\pm 2.62$ meV
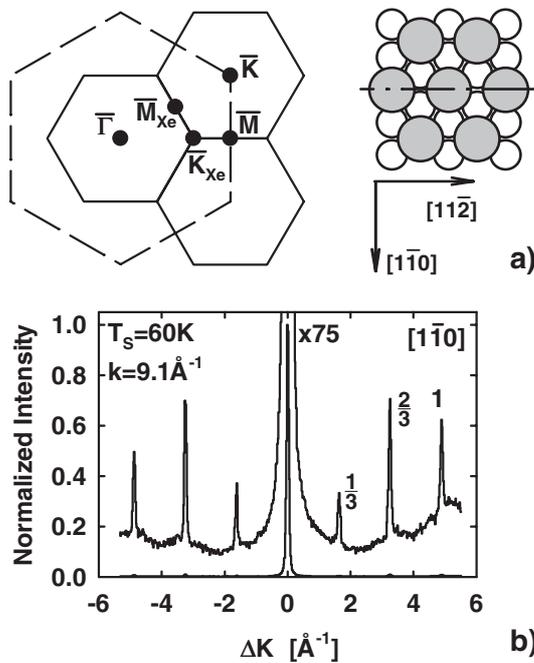
**Figure 3.** (*a*) Right panel: the structure of the $(\sqrt{3} \times \sqrt{3})$R30° monolayer of Xe atoms (shaded circles) on a Cu(111) surface, with examples of two high-symmetry directions (azimuths) in the substrate surface plane. Left panel: two-dimensional BZs of the Cu(111) surface (dashed lines) and of the Xe adlayer (full lines). (*b*) He-atom angular distribution along the [1$\bar{1}$0] azimuth of the substrate from the $(\sqrt{3} \times \sqrt{3})$R30° Xe monolayer on Cu(111) for incident wavevector $k_i = 9.2$ Å$^{-1}$ ($E_i = 45$ meV) and surface temperature 60 K.

on the energy loss and gain sides of the TOF spectrum, respectively. Within the experimental error these energies do not change in the interval between $\Delta K = 0.1$ and $0.3$ Å of the first SBZ of the superstructure in which the signal was detectable. In accordance with previous works on noble-gas atoms adsorbed on other substrates [33–35], this mode was assigned to the excitation of collective vibrations of Xe atoms with a polarization vector vertical to the surface and designated the 'S-mode'. The lack of dispersion indicates that the frequency of the vertically polarized phonon is mainly determined by the adsorbate coupling to the substrate, with only a weak coupling to adjacent adsorbates. Deviation from a dispersionless behaviour occurs only at the intersection with the substrate Rayleigh mode [35, 36]. The energy of this Einstein-like or S-mode ($\hbar\omega_0 = \hbar\omega_S = 2.62$ meV [25–27]) is slightly larger than for the (110) face of Cu ($\hbar\omega_S = 2.5$ meV [37]). The small but significant deviation of 0.12 meV is consistent with a slightly deeper potential well for Xe on Cu(111) and Cu(001) (in the latter case $\hbar\omega_S = 2.71$ meV [25, 26]) than on Cu(110) [38, 39].

In addition to the intense S-peaks, the measured He $\rightarrow$ Xe/Cu(111) spectrum also reveals the presence of a weak but clearly resolved feature (labelled 'L') near the elastic or zero-energy loss line. The energy of this mode changes with the angle of incidence $\theta_i$ and thus shows dispersion. The relative intensity of this mode was found to decrease strongly with the wavevector, so the corresponding data points could only be obtained for parallel wavevector up to one third of the distance between the $\bar{\Gamma}$ and $\bar{K}_{Xe}$ points in the first BZ of the superstructure. Since in the TOF spectra displayed the energy of the L-mode is always significantly below that of the lowest surface phonon of the clean Cu(111) surface, this must be a pure Xe adlayer-
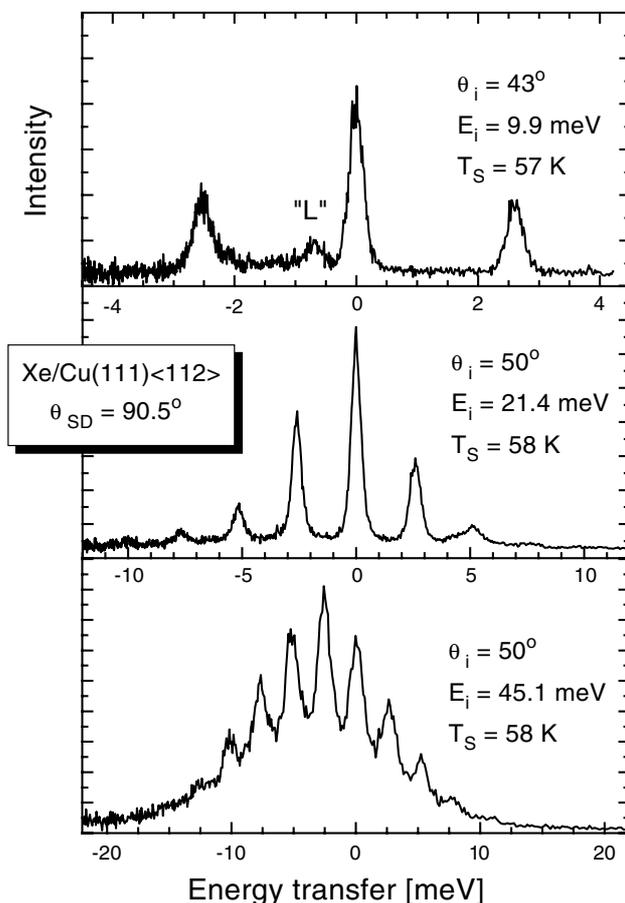
**Figure 4.** A series of measured HAS TOF spectra for a monolayer of Xe on Cu(111) along the [11$\bar{2}$] direction of the substrate surface for three representative He-atom incident energies. $\theta_i$ and $\theta_{SD}$ denote the angle of incidence and the fixed total scattering angle, respectively. The scattering parameters are shown in the insets.

induced mode which cannot couple to the substrate for wavevectors over a wide range of the SBZ. Since for the $(\sqrt{3} \times \sqrt{3})$R30° Xe/Cu(111) system the [11$\bar{2}$] direction has a high-symmetry mirror plane, the vibrational modes are partitioned into two orthogonal classes [32]. Two thirds of the modes are polarized in the sagittal plane (including the adlayer-induced S- and L-modes). The remaining one third of the modes are polarized in the surface plane and normal to the mirror plane and designated shear horizontal modes or 'SH-modes'. The three possible adlayer-induced orthogonal modes with the wavevector in the [11$\bar{2}$] direction (cf figure 3(*a*)) are thus characterized by either a combination of the components with S- and L-polarization or pure SH-polarization. Combining the symmetry selection rules pertinent to the probabilities of excitation of in-plane phonons at ideal surfaces [14, 16] with the fact that the data were recorded in the first SBZ of the superstructure and in the sagittal plane which coincides with the high-symmetry plane of the Xe/Cu(111) system, the observation of the SH-mode under these experimental conditions can be ruled out. Hence, this mode is tentatively assigned to the longitudinal mode of the adlayer which is known to couple to the scattered He atoms under similar conditions [14, 17]. However, as demonstrated for NaCl, the SH-modes *can* be excited along a high-symmetry direction in the *second* SBZ [40].
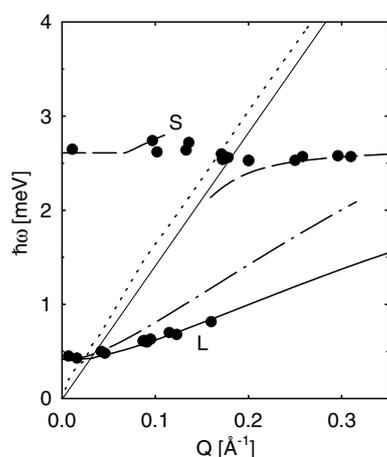
**Figure 5.** Phonon dispersions for the Xe/Cu(111) surface along the $[11\bar{2}]$ direction relative to the substrate as determined by HAS (full circles). The solid line denotes the best fit achieved for the longitudinal (L) mode in the Xe adlayer and the dashed–dotted curve is the result for the L-mode using the gas-phase Xe–Xe potential. The theoretical dispersion curve for the vertically polarized S-mode is marked by the long-dashed curve and that of the Rayleigh phonon and the projected bulk phonon edge of the Cu substrate by the full thin and dotted lines, respectively. For the force constants, see table 1.

The other two spectra in figure 4 demonstrate the transition from a single-phonon to a multiphonon scattering regime as $E_i$ is increased. This transition takes place already at rather low He-atom incident energies due to the very low excitation energies of the adlayer-induced S-modes whose vertical polarization gives rise to a strong projectile–phonon coupling. Although some single-phonon features are still discernible at incident energy $E_i = 21.4$ meV, both spectra are dominated by a number of uniformly spaced peaks at energies $\pm n \times 2.62$ meV. For $E_i = 45.1$ meV the true multiphonon scattering regime is reached because the intensity of the elastic peak is smaller than that of the multi-quantum S-peak for $n = 2$.

It is noteworthy that the S-mode multiphonon lines are all, to within experimental error, located at integral multiples of a fundamental frequency, $\omega_S = 2.6$–$2.7$ meV/$\hbar$. At first sight this seems to imply a very harmonic Xe–Cu potential since anharmonic shifts, which are expected to be negative, would produce overtone energies smaller than the corresponding multiples of the fundamental frequency $\omega_S$. However, the theoretical analyses of the Xe–metal interactions [38, 39, 41] show that the potential is highly anharmonic but, as is demonstrated below, the multiple spectral peaks can be explained by multiple excitation of delocalized phonon modes which involve the lowest harmonic states of many adatoms rather than a single higher anharmonic state localized on a single adatom. In this case there appears no anharmonic shift as each multiphonon excitation is distributed over the Xe atoms in the adlayer.

The experimentally determined dispersion curves are shown in figure 5. The vertically polarized S-mode exhibits negligible dispersion over the major part of the SBZ except at the point of avoided crossing with the substrate RW [33, 34]. The L-mode for the commensurate Xe/Cu(111) structure exhibits a zone-centre gap of about 0.5 meV [27]. In order to corroborate the assignments of the modes in the He $\rightarrow$ Xe/Cu(111) TOF spectra and theoretically analyse their dispersion and excitation intensities, a full lattice dynamics calculation of the vibrationally coupled $(\sqrt{3} \times \sqrt{3})$R30° Xe/Cu(111) system has been carried out. In view of independent experimental evidence [29], the Xe atoms were placed in on-top sites on both sides of a 40-layer-thick slab of substrate atoms. The interaction between nearest-neighbour Cu atoms was

**Table 1.** The values of the radial, $\beta_1$, and tangential, $\alpha_1$, force constants for the first-nearest neighbours used in the analysis of phonon dispersion curves of the commensurate Xe/Cu(111) system. Note a significant softening of $\beta_1^{Xe-Xe}$ relative to the value of 1.67 N m$^{-1}$ obtained using gas-phase Xe–Xe HFD-B2 potentials [43]. In this system Xe atoms are adsorbed in a $(\sqrt{3} \times \sqrt{3})R30°$ superstructure on top of Cu atoms [29].

| Force constant (commensurate Xe/Cu(111) system) | Value (N m$^{-1}$) |
| --- | --- |
| $\beta_1^{Cu-Cu}$ | 28.0 |
| $\beta_1^{Cu-Xe}$ | 3.7 |
| $\alpha_1^{Cu-Xe}$ | 0.086 |
| $\beta_1^{Xe-Xe}$ | 0.5 |
| $\alpha_1^{Xe-Xe}$ | 0 |

accounted for by a single radial force constant $\beta_1^{Cu-Cu} = 28.0$ N m$^{-1}$ as obtained from a fit of the bulk Cu phonon dispersion curves [42]. The other parameters describing the coupling of Xe atoms to the nearest-neighbour Cu substrate atoms was fitted to the dispersion curves, which yielded a radial force constant $\beta_1^{Cu-Xe} = 3.7$ N m$^{-1}$ and a tangential force constant $\alpha_1^{Cu-Xe} = 0.086$ N m$^{-1}$. Assigning the longitudinal character to the observed L-mode to comply with the above-discussed symmetry selection rules, the interaction between the atoms in the adlayer could be described by a radial force constant $\beta_1^{Xe-Xe} = 0.5$ N m$^{-1}$ and a tangential force constant $\alpha_1^{Xe-Xe} = 0$. The values of these force constants are presented in table 1. The results of the full dynamical matrix calculation for the dispersion of the surface-projected S- and L-modes are also shown in figure 5 and they reproduce the experimental data very satisfactorily. The radial Xe–Xe force constant $\beta_1^{Xe-Xe} = 0.5$ N m$^{-1}$ resulting from this procedure is, however, significantly smaller than the value predicted from the highly precise HFD-B2 gas-phase potential [43], $\beta_{HFD}^{Xe-Xe} = 1.67$ N m$^{-1}$, which produces a significantly steeper dispersion curve for longitudinal phonons denoted by the dash–dotted curve in figure 5. The complete results of the present dynamical matrix calculation for phonon dispersion in the Xe/Cu(111) system are shown in figure 6(a). This calculation also enables us to trace how each phonon mode of the composite system is localized at the surface (i.e. within the adlayer) and how the typical surface modes may become delocalized for certain values of the wavevector. A measure of the adlayer localization of the S-, L-, and SH-modes near the centre of the first BZ of the superstructure is shown in figure 6(b). Further important information concerning the percentage of vertical component of polarization of the L-mode in the same region, indicating the mode ellipticity, is illustrated in figure 6(c). However, the physical origin of the unexpected large softening of the radial Xe–Xe force constants introduced to reconcile the symmetry requirements with the experimental data remains unclear. A clue to this effect may be provided by the peculiar electronic structure of the Cu(111) surface which supports surface electronic states with corresponding electronic wavefunctions extending far across the adsorbed Xe atoms [44].

In the present approach the calculation of the matrix elements of the projectile–phonon interaction in expression (8) is based on the pairwise summation of projectile–adsorbate pair pseudopotentials $v(r_{He} - r_{Xe})$ described in detail in [16] and [25]. The two-dimensional Fourier transform of the pair pseudopotential, $v(Q, z)$, is modelled by a Morse potential [16, 25]:

$$v(Q, z) = A_c D[e^{-2\beta(z-z_m)}e^{-Q^2/2Q_c^2} - 2e^{-\beta(z-z_m)}e^{-Q^2/Q_c^2}]. \tag{21}$$

Here the parameters $D$, $\beta$, and $z_m$ are listed in table 2, $A_c$ denotes the area of the unit cell of the superstructure, and the cut-off wavevector is given by $Q_c = \sqrt{2\beta/z_t}$ where $z_t$ is the value of the projectile atom turning point in the averaged static projectile–surface potential $U_0(z)$ consistent with expression (21). This potential is given by
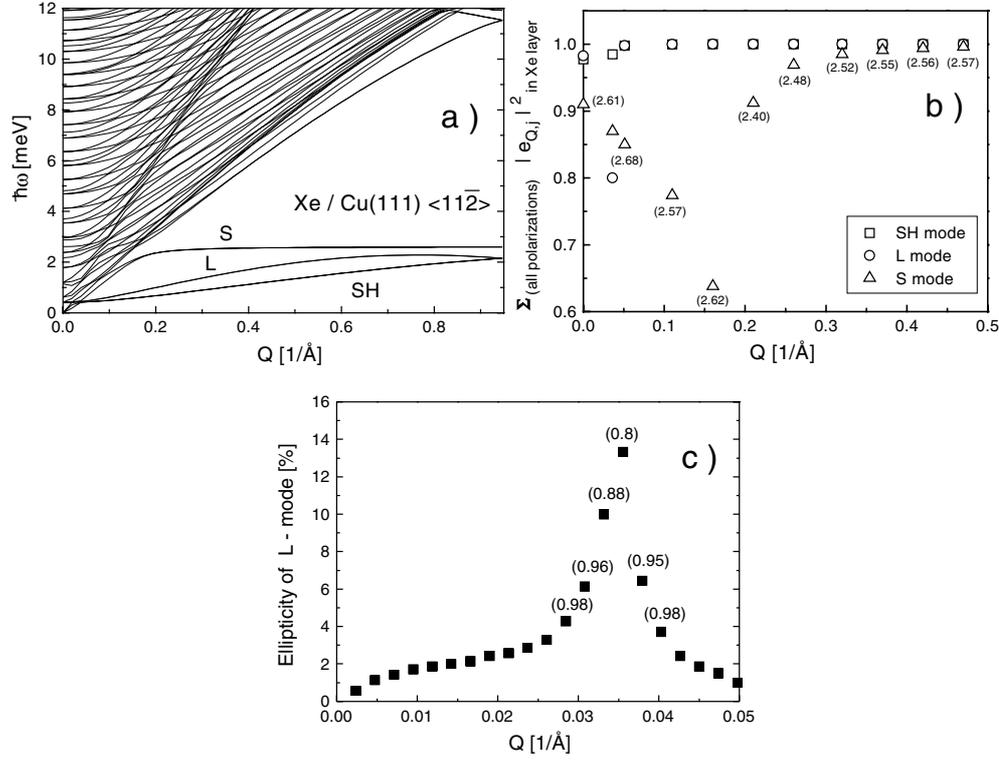
**Figure 6.** (*a*) Dispersion curves for the Xe/Cu(111) system along the [11$\bar{2}$] direction calculated using the dynamical matrix approach to a slab of 40 Cu layers with Xe atoms in on-top positions on each side. For the force constants, see table 1. Note that the S-, L-, and SH-mode dispersion curves are detached from the bulk quasi-continuum. (*b*) Surface localization of Xe-induced S-, L-, and SH-modes on the adlayer expressed through the sum of components of the respective polarization vectors in the adlayer. Numbers below the symbols △ denote frequencies (in meV) of the S-mode. (*c*) Percentage of vertical polarization of the L-mode in the Xe adlayer on the Cu(111) substrate, or L-mode ellipticity, as a function of the L-phonon wavevector. Numbers in parentheses above the full squares denote the fractional adlayer localization of the L-mode.

$$U_0(z) = D\{\exp[-2\beta(z - z_m)] - 2\exp[-\beta(z - z_m)]\}. \tag{22}$$

Using the formulae for calculation of inelastic scattering intensities described in the preceding section and expressions (21) and (22) for the pseudopotentials, one can proceed with the evaluation of scattering spectra for comparison with the experimental data available for the He → Xe/Cu(111) collision system. The theoretical spectra have been additionally convoluted by a Gaussian whose width amounts to 2% of the incoming beam energy. This mimics the overall experimental resolution of the HAS TOF apparatus on which the experiments have been carried out [25–27]. A comparison of the experimental and the thus-calculated spectral intensities of the L- and S-modes (including the EBA correction for the S-phonon intensities [16,28]) in the single-phonon scattering regime of HAS from Xe/Cu(111) is shown in figure 7. Here the component due to elastic diffuse scattering from defects, not accounted for by the scattering formalism described in section 2, has been modelled by a Gaussian of the height that together with the calculated elastic peak intensity matches the height of the experimental elastic peak. This aids comparison of the calculated L-peak intensities with experiment because the finite width of the elastic peak can also contribute to the background intensity of the L-peaks
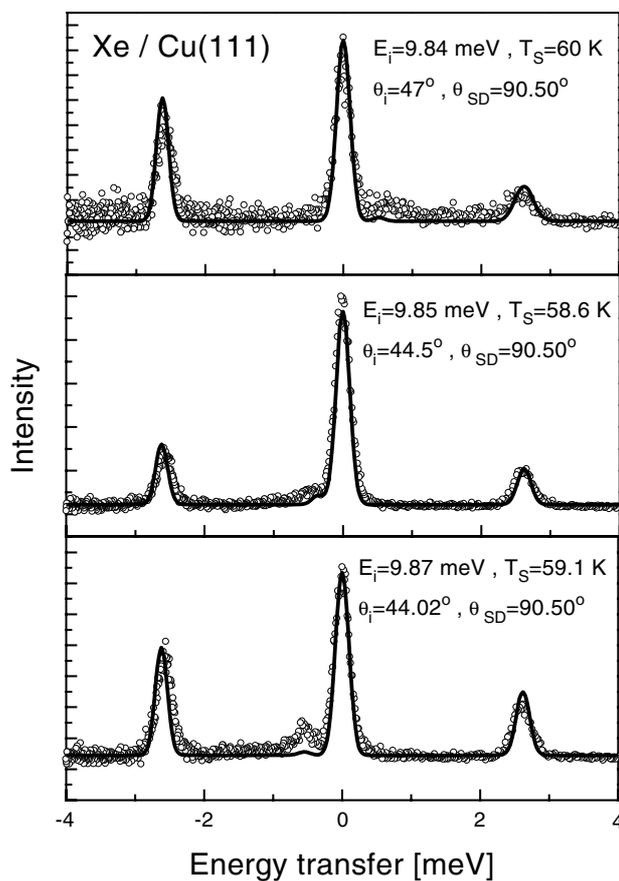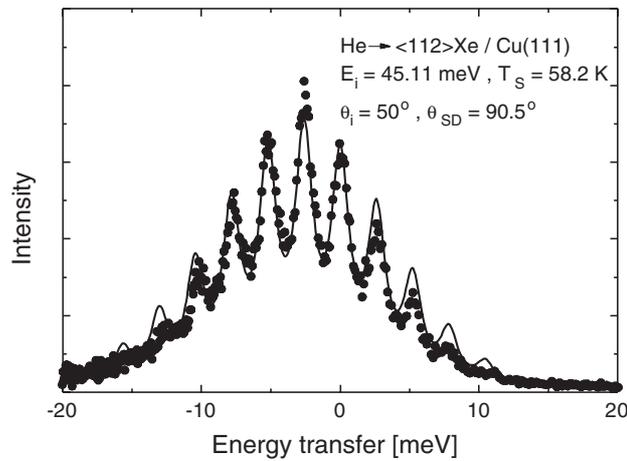
**Figure 7.** Comparison of experimental and calculated S- and L-mode intensities in the single-phonon scattering spectra typical of He → Xe/Cu(111) collisions.

**Table 2.** Parameters for the best-fit Morse potentials $v(Q, z)$ and $U_0(z)$, equations (21) and (22), respectively, for modelling the He-atom interaction with the Xe/Cu(111) surface.

| $D$ (meV) | $\beta^{-1}$ (Å) | $z_m$ (Å) |
|-----------|------------------|-----------|
| 6.60      | 0.8202           | 3.49      |

measured close to the no-loss line. With this proviso, a good agreement between experimental and theoretical results is achieved, which illustrates the consistency of the present interpretation of the inelastic peaks in the HAS TOF spectra from Xe/Cu(111) surface.

As the coupling of He atoms to S-modes is much stronger than that to the L-modes [14, 16, 17], the multiphonon scattering spectra will be dominated by a series of multi-quantum S-peaks. All other dispersive modes may only add weak structures on top of this basic one. Eventually, these structures will turn into a Gaussian-like background [16] in the limit of high incident projectile energies. The multiphonon scattering spectra from Xe/Cu(111) adlayers have been studied in detail in [25] and [26]. Figure 8 shows a comparison of experimental data with the EBA multiphonon spectrum calculated by consistently employing the potentials from the corresponding single-phonon calculations. The multiphonon He → Xe/Cu(111)

**Figure 8.** Comparison of experimental and calculated EBA multiphonon scattering spectra typical of He → Xe/Cu(111) collisions using the same potentials and dispersion relations as in figure 7.

spectrum can be viewed as a convolution of a series of well-defined equidistant peaks, signifying the uncorrelated multiple emission and absorption of nondispersive S-phonons (and not the overtones [25]), superimposed on a background arising from the multiple excitation of L- and also SH-phonons which outside the one-phonon scattering regime are no longer constrained by the symmetry selection rules.

## 4. Kinematic effects in the intensities of inelastic transitions in He → Xe/Cu(111) collisions

The comparison of experimental and theoretical HAS intensities displayed in figures 7 and 8 is very satisfactory and hence provides a test of the reliability of the model developed in section 2 for the description of inelastic He → Xe/Cu(111) scattering. This enables us to use the thus-verified theoretical approach to investigate the effects of kinematic factors on inelastic collisions and sticking processes in the collision system He → Xe/Cu(111) under the various scattering conditions. To this end we have examined the behaviour of the DWE (14) (and thereby also of the scattering function (7)) in the various collision regimes, as this provides important information on the effects of kinematic factors on the magnitude of integrated quantities relevant to the description of inelastic scattering.

Figures 9(*a*) and (*b*) show the calculated dependence of the DWE, equation (14), on the incident energy of He atoms scattered from the Xe/Cu(111) surface at the temperature $T_s = 0$. In the zero-temperature limit all the sticking processes are phonon-emission-assisted processes and are prompt (i.e. $E_f - E_i < 0$ in equations (4) and (12)) and hence the kinematic effects associated with one-phonon emission processes are easily discernible. In view of the earlier finding that the contribution of S-phonons to the inelastic scattering spectra is by far the most dominant one (cf [16]), we have taken into account in the present calculation of the DWE only the projectile coupling to S-phonons. The calculations have been carried out for $\theta_i = 50°$ (figure 9(*a*)) and $\theta_i = 0$ (figure 9(*b*)), i.e. the incident angles for which the singular properties of the energy-conserving $\delta$-functions in equation (19) were examined and illustrated in figure 1. As is clearly seen in these plots, the magnitude of the DWE at low incoming energies ($E_i < 6$ meV) is strongly affected by the c–b transitions. The two maxima in $2W_{k_i,T_s}^{c-b}$ appear
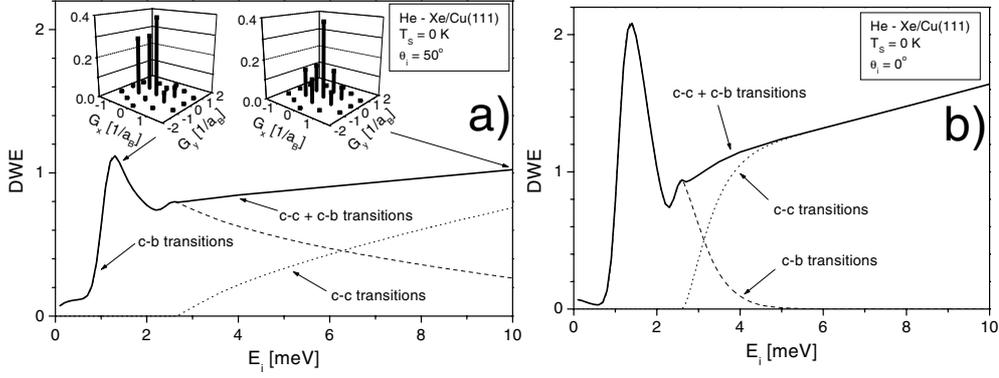
**Figure 9.** Plots of the DWE (equation (14)) shown as a function of He-atom incident energy $E_i$ and at zero substrate temperature, for two incoming angles (*a*) $\theta_i = 50°$ and (*b*) $\theta_i = 0°$. Contributions from c–c and c–b transitions are denoted by short-dashed and long-dashed curves, respectively. Insets in (*a*) indicate relative contributions to the DWE from different parts of the SBZ at low incident energies when only the c–b transitions are possible, and at higher incident energies when the c–c transitions dominate. Note that in the case of normal incidence $\theta_i = 0°$, contributions from all directions of the SBZ give equal contributions to the DWE.

at $E_i = \epsilon_n + \hbar\omega_S$, for $\epsilon_2 = -0.132$ meV (smaller maximum) and $\epsilon_1 = -1.551$ meV (larger maximum), whereas the bound state $\epsilon_0 = -4.528$ meV is inaccessible through emission of a single phonon quantum $\hbar\omega_S = 2.62$ meV. The drop of $2W_{k_i,T_s}^{c-c}$ to zero for $E_i < 6$ meV in figure 9(*b*) is a consequence of the fully quantum treatment of the scattering event. This is in contrast to the recoilless trajectory approximation (TA) calculations in which this feature is absent (cf the discussion following figure 4 in [22]). The analogous drop in figure 9(*a*) is much slower due to the less-stringent conditions on the phase space of allowed final-state quantum numbers in the case of non-normal incidence of the projectile. The insets in figure 9(*a*) illustrate that for c–b transitions at low $E_i$ and non-normal projectile incidence, the preferred parallel momentum exchange $\Delta K$ with phonons is directed (i.e. effectively focused) towards negative values, whereas at higher $E_i$ when the c–c transitions prevail this trend is much less pronounced. The behaviour of $2W_{k_i,T_s}^{c-c}$ in the interval $E_i > 6$ meV, in which it starts growing linearly with $E_i$, is an expected manifestation of the behaviour of interaction matrix elements which tend to a semiclassical limit as $E_i$ is increased.

Comparison of figures 9(*a*) and (*b*) reveals another interesting feature. Inspection of the magnitudes of c–c contributions to the DWE shows that at higher incident energies they scale as $2W_{k_i,T_s}^{c-c}(\theta_i = 50°, E_i) \simeq 2W_{k_i,T_s}^{c-c}(\theta_i = 0, E_i \cos^2 \theta_i)$, as one may expect in the semiclassical limit. However, this ceases to be so for the *c–b* transitions because of a very different effect of kinematic factors on $2W_{k_i,T_s}^{c-b}$. As is evident from comparison of the values of DWE at $E_i = \epsilon_1 + \hbar\omega_S$ in figures 9(*a*) and (*b*), the different kinematic conditions give rise to different *final-state* focusing effects and thereby to different values of $2W_{k_i,T_s}^{c-b}$ which, in turn, do not follow a simple scaling behaviour.

## 5. Summary

Taking the example of a prototype monolayer system Xe/Cu(111), whose surface vibrational modes with Einstein and Debye types of dispersion have been extensively studied by means of HAS, we have investigated how the kinematic conditions affect the magnitude of integrated quantities which play a fundamental role in the interpretations of phonon-mediated inelastic

atom–surface scattering and sticking processes. We have shown that in the case of energy transfer from the projectile particle to nondispersive Einstein phonons, the prompt sticking coefficients are strongly affected by the focusing effects in the scattered channels and that these effects are sensitive to the initial kinematic conditions. This phenomenon manifests itself in specific low-energy behaviour of the DWE and the DWF as the projectile energy and angle of incidence are varied. The results of a detailed quantum mechanical calculation of the DWE for the He → Xe/Cu(111) collision system carried out in section 3 and shown in figure 9 clearly demonstrate the focusing-induced deviations from the semiclassical behaviour that is often uncritically invoked in interpretations of HAS experiments.

## Acknowledgments

## References

[1] Benedek G 1975 *Phys. Rev. Lett.* **35** 234
[2] See the articles in: Hulpke E (ed) 1992 *Helium Atom Scattering From Surfaces (Springer Series in Surface Sciences vol 27)* (Berlin: Springer)
[3] Benedek G, Brusdeylins G, Doak R B, Skofronick J G and Toennies J P 1983 *Phys. Rev.* B **28** 2104
[4] Lock A, Toennies J P, Wöll Ch, Bortolani V, Franchini A and Santoro G 1988 *Phys. Rev.* B **37** 7087
[5] Benedek G, Gerlach R, Glebov A, Lange G, Miret-Artés S, Skofronick J G and Toennies J P 1996 *Phys. Rev.* B **53** 11 211 and references therein
[6] Glebov A, Manson J R, Miret-Artés S, Skofronick J G and Toennies J P 1998 *Phys. Rev.* B **57** R9455
[7] Doak R B 1992 *Atomic and Molecular Beam Methods* vol 2, ed G Scoles (New York: Oxford University Press) section 14
[8] Miret-Artés S and Manson J R 1999 *Phys. Rev.* B **60** 6080
[9] Brusdeylins G, Doak R B and Toennies J P 1981 *J. Chem. Phys.* **75** 1784
[10] Miret-Artés S 1996 *Surf. Sci.* **366** L735 and references therein
[11] Miret-Artés S 1999 *Phys. Rev.* B **60** 1547
[12] Šiber A, Gumhalter B, Graham A P and Toennies J P 2001 *Phys. Rev.* B **63** 115411
[13] Miret-Artés S and Manson J R 2001 *Phys. Rev.* B **63** 121404
[14] Celli V 1991 *Surface Phonons (Springer Series in Surface Sciences vol 21)* ed W Kress and F W de Wette (Berlin: Springer)
[15] For definitions and characteristics of surface Rayleigh wave and longitudinal resonance phonons see articles in: Kress W and de Wette F W (ed) 1991 *Surface Phonons (Springer Series in Surface Sciences vol 21)* (Berlin: Springer)
[16] Gumhalter B 2001 *Phys. Rep.* **351** 1
[17] Santoro G and Bortolani V 1993 *Inelastic Energy Transfer in Interactions with Surfaces and Adsorbates* ed B Gumhalter, A C Levi and F Flores (Singapore: World Scientific) p 1
[18] Brunner Th and Brenig W 1993 *Surf. Sci.* **291** 192
Brunner Th and Brenig W 1993 *Inelastic Energy Transfer in Interactions with Surfaces and Adsorbates* ed B Gumhalter, A C Levi and F Flores (Singapore: World Scientific) p 95
[19] Brivio G P and Grimley T B 1993 *Surf. Sci. Rep.* **17** 1
[20] Burke K, Gumhalter B and Langreth D C 1993 *Phys. Rev.* B **47** 12 852
[21] Gumhalter B, Burke K and Langreth D C 1994 *Surf. Rev. Lett.* **1** 133
[22] Bilić A and Gumhalter B 1995 *Phys. Rev.* B **52** 12 307
[23] Gumhalter B 1996 *Surf. Sci.* **347** 237
[24] Šiber A and Gumhalter B 1998 *Phys. Rev. Lett.* **81** 1742
[25] Šiber A, Gumhalter B, Braun J, Graham A P, Bertino M F, Toennies J P, Fuhrmann D and Wöll Ch 1999 *Phys. Rev.* B **59** 5898
[26] Braun J, Fuhrmann D, Graham A P, Toennies J P, Wöll Ch, Bilić A and Gumhalter B 1997 *J. Chem. Phys.* **106** 9911

[27]  Braun J, Fuhrmann D, Šiber A, Gumhalter B and Wöll Ch 1998 *Phys. Rev. Lett.* **80** 125
[28]  Gumhalter B, Šiber A and Toennies J P 1999 *Phys. Rev. Lett.* **83** 1375
[29]  Seyller Th, Caragiu M, Diehl R D, Kaukasoina P and Lindroos M 1998 *Chem. Phys. Lett.* **291** 567
[30]  Chesters M A, Hussain M and Pritchard J 1973 *Surf. Sci.* **35** 161
[31]  Jupille J, Erhardt J-J, Fargues D and Casuto A 1990 *Faraday Discuss. Chem. Soc.* **89** 323
      Jupille J, Erhardt J-J, Fargues D and Casuto A 1990 *Vacuum* **41** 399
[32]  Wöll Ch 1991 *Appl. Phys.* A **53** 377
[33]  Hall B, Mills D L and Black J E 1985 *Phys. Rev.* **32** 4932
[34]  Gibson K D, Sibener S J, Hall B M, Mills D L and Black J E 1985 *J. Chem. Phys.* **83** 4256
[35]  Hall B, Mills D L, Zeppenfeld P, Kern K, Becher U and Comsa G 1989 *Phys. Rev.* B **40** 6326
[36]  Harten U, Toennies J P and Wöll Ch 1985 *Faraday Discuss. Chem. Soc.* **80** 137
[37]  Zeppenfeld P, Büchel M, David R, Comsa G, Ramseyer C and Giradet C 1994 *Phys. Rev.* B **50** 14 667
[38]  Vidali G, Ihm G, Kim H-Y and Cole M W 1991 *Surf. Sci. Rep.* **12** 133
[39]  Chizmeshya A and Zaremba E 1992 *Surf. Sci.* **268** 432
[40]  Glebov A, Silvestri W, Toennies J P, Benedek G and Skofronick J G 1996 *Phys. Rev.* B **54** 17 866
[41]  Lang N D 1981 *Phys. Rev. Lett.* **46** 842
      Lang N D and Williams A R 1982 *Phys. Rev.* B **25** 2940
[42]  Ellis J, Toennies J P and Witte G 1995 *J. Chem. Phys.* **102** 5059
[43]  Aziz R A and Slaman M J 1986 *Mol. Phys.* **58** 679
      Dham A K, Allnatt A R, Meath W J and Aziz R A 1989 *Mol. Phys.* **67** 1291
      Dham A K, Meath W J, Allnatt A R, Aziz R A and Slaman M J 1990 *Chem. Phys.* **142** 173
[44]  Wolf M, Knoesel E and Hertel T 1996 *Phys. Rev.* B **54** R5295